Inorganic Chemistry

Article

pubs.acs.org/IC

Rich Structural Chemistry in New Alkali Metal Yttrium Tellurites: Three-Dimensional Frameworks of $NaYTe_4O_{10}$, $KY(TeO_3)_2$, $RbY(TeO_3)_2$, and a Novel Variant of Hexagonal Tungsten Bronze, $CsYTe_3O_8$

Youngkwon Kim, Dong Woo Lee, and Kang Min Ok*

Department of Chemistry, Chung-Ang University, 84 Heukseok-ro, Dongjak-gu, Seoul 156-756, Republic of Korea

Supporting Information

ABSTRACT: Pure polycrystalline phases and single crystals of four new quaternary alkali metal yttrium tellurites, $NaYTe_4O_{10}$, $KY(TeO_3)_2$, $RbY(TeO_3)_2$, and $CsYTe_3O_8$, have been prepared by solid-state and hydrothermal reactions using A_2CO_3 (A = Na, K, Rb, and Cs), $Y(NO_3)_3 \cdot 6H_2O$, Y_2O_3, and TeO_2 as starting reagents. X-ray diffraction analyses suggest that $NaYTe_4O_{10}$ exhibits a highly symmetric three-dimensional (3D) framework consisting of YO_8 square antiprisms and chains of TeO_4 polyhedra. Within the framework, six- (6-) and eight-membered ring (8-MR) channels are observed. $KY(TeO_3)_2$ and $RbY(TeO_3)_2$ are isostructural to each other and reveal another 3D framework with structures containing YO_6 octahedra and TeO_3 trigonal pyramids with 4-MR and 12-MR channels. $CsYTe_3O_8$ shows a hexagonal tungsten bronze (HTB)-like topology composed of hexagonal tungsten oxide-like layers of TeO_4 polyhedra and YO_6 octahedral linkers with 3-MR and 6-MR channels. Thermal analyses, elemental analyses, and spectroscopic characterizations, such as UV–vis diffuse reflectance and infrared spectra, are presented, as are local dipole moment calculations for the constituent asymmetric polyhedra TeO_3 and TeO_4.

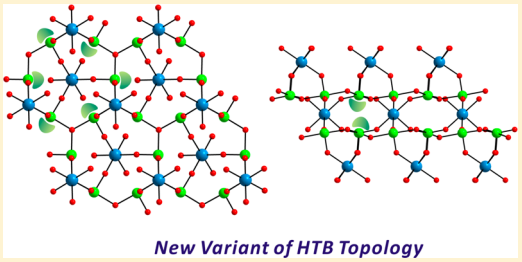

INTRODUCTION

Tellurites (i.e., Te^{4+} oxides crystallized with a variety of metal cations) often reveal rich and enchanting chemistry. Mixed-metal tellurites are generally prepared through various synthetic methods, which include solid-state and solvothermal reactions.[1] The oxide itself (i.e., tellurium dioxide (TeO_2) with an accessible melting point of 733 °C) is extremely versatile as a starting material due to its superior reactivity with other nonreactive oxides, easy availability as a flux for crystal growth, and excellent solubility in many solvents in the presence of appropriate mineralizers.[2] The coordination environment of Te^{4+} in mixed-metal tellurium oxides is of particular interest. Te^{4+} is coordinated to 3-, 4-, and 5-oxide ligands and exhibits as TeO_3, TeO_4, and TeO_5 polyhedra, respectively. In fact, a variety of framework dimensions and rich structural chemistries found in tellurites with extended structures are attributable to the flexible coordination mode of Te^{4+}.[3] In addition, Te^{4+} is consistently witnessed in an unsymmetrical environment that can be attributed to its nonbonded electron pair. The stereoactive lone pair on the cation is considered to be the result of mixing between the metal s and oxygen p orbitals through a second-order Jahn–Teller effect.[4] Once the locally unsymmetrical building block is well-aligned, interesting symmetry dependent characteristics such as ferroelectric, multiferroic, pyroelectric, piezoelectric, and nonlinear second-order properties can be expected.[5] Thus far, a number of noncentrosymmetric (NCS) mixed-metal tellurites have been discovered through exploratory syntheses using the Te^{4+} cation.[6] Meanwhile, a peculiar geometric form that is often found in NCS materials is the three-dimensional (3D) hexagonal tungsten bronze (HTB) framework, in which the backbone is composed of corner-shared MO_6 octahedra.[7] Within the hexagonal network of MO_6 octahedra, an array of three- (3-) and six-membered rings (6-MRs) is observed. A similarly related two-dimensional structure is hexagonal tungsten oxide (HTO) geometry, in which the layers are normally capped by polyhedra of cations, such as P^{5+}, Te^{4+}, Se^{4+}, and Sb^{3+}.[8] We have been very interested in exploring the $A^+–Y^{3+}–Te^{4+}–$oxide system to discover novel quaternary tellurites. To our surprise, only two ternary tellurites ($Y_2Te_4O_{11}$ and $Y_2Te_5O_{13}$),[9] one quaternary tellurite ($Y_2MoTe_3O_{12}$),[10] and one yttrium tellurite chloride $[Na_2YCl_3(TeO_3)_4]$[11] have been reported to date. Interestingly, $Y_2Te_5O_{13}$, $Y_2MoTe_3O_{12}$, and $Na_2YCl_3(TeO_3)_4$ exhibit layered structures, whereas $Y_2Te_4O_{11}$ reveals a 3D framework topology. Our exploratory synthetic approaches through solid-state and hydrothermal reactions result in four new quaternary alkali metal yttrium tellurites, $NaYTe_4O_{10}$, $KY(TeO_3)_2$, $RbY(TeO_3)_2$, and $CsYTe_3O_8$. Whereas the tellurites $NaYTe_4O_{10}$, $KY(TeO_3)_2$, and $RbY(TeO_3)_2$ exhibit 3D frameworks with several different channels, $CsYTe_3O_8$ shows a novel HTB-like framework. To the best of our knowledge, $CsYTe_3O_8$ is the first example of an HTB-like topological variant that consists of HTO-like layers of TeO_4 polyhedra and YO_6 octahedral linkers. Thorough spectroscopic, elemental, and thermal characterizations are

Received: November 12, 2014
Published: December 17, 2014

presented, as are dipole moment calculations for the component unsymmetrical polyhedra.

EXPERIMENTAL SECTION

Reagents. Na_2CO_3 (Hayashi, 99.5%), K_2CO_3 (Jin Chemical, 99.5%), Rb_2CO_3 (Alfa Aesar, 99.8%), Cs_2CO_3 (Aldrich, 99%), $Y(NO_3)_3{\cdot}6H_2O$ (Alfa Aesar, 99.8%), Y_2O_3 (Alfa Aesar, 99.9%), and TeO_2 (Alfa Aesar, 99%) were used as received.

Syntheses. Crystals of all of the reported materials were grown through hydrothermal reactions. For $NaYTe_4O_{10}$, 0.318 g (3.00×10^{-3} mol) of Na_2CO_3, 0.383 g (1.00×10^{-3} mol) of $Y(NO_3)_3{\cdot}6H_2O$, 0.239 g (1.50×10^{-3} mol) of TeO_2, and 0.5 mL of water were combined. For $KY(TeO_3)_2$, 0.415 g (3.00×10^{-3} mol) of K_2CO_3, 0.383 g (1.00×10^{-3} mol) of $Y(NO_3)_3{\cdot}6H_2O$, 0.239 g (1.50×10^{-3} mol) of TeO_2, and 0.5 mL of water were combined. For $RbY(TeO_3)_2$, 0.693 g (3.00×10^{-3} mol) of Rb_2CO_3, 0.383 g (1.00×10^{-3} mol) of $Y(NO_3)_3{\cdot}6H_2O$, 0.239 g (1.50×10^{-3} mol) of TeO_2, and 0.5 mL of water were combined. For $CsYTe_3O_8$, 0.977 g (3.00×10^{-3} mol) of Cs_2CO_3, 0.383 g (1.00×10^{-3} mol) of $Y(NO_3)_3{\cdot}6H_2O$, 0.239 g (1.50×10^{-3} mol) of TeO_2, and 1.0 mL of water were combined. Each reaction mixture was transferred to 23 mL Teflon-lined autoclaves that were tightly sealed. The reactors were heated to 230 °C for 4 days and were cooled to room temperature at 6 °C h^{-1}. The reaction products were recovered by filtration and washed several times with water. Colorless crystals of $NaYTe_4O_{10}$, $KY(TeO_3)_2$, $RbY(TeO_3)_2$, and $CsYTe_3O_8$ were isolated in 55, 56, 49, and 62% yields, respectively, based on $Y(NO_3)_3{\cdot}6H_2O$. Although single phase crystals of $NaYTe_4O_{10}$, $KY(TeO_3)_2$, and $RbY(TeO_3)_2$ were successfully obtained from hydrothermal reactions, crystals of $CsYTe_3O_8$ were isolated along with polycrystalline phases of Cs_2TeO_4 (powder diffraction file (PDF): 49-1847) and $Y_2Te_4O_{11}$ (PDF: 35-1162). Thus, attempts have been made to synthesize pure phases of polycrystalline samples for the reported materials through standard solid-state reactions. Stoichiometric amounts of corresponding alkali metal carbonates, Y_2O_3, and TeO_2 were thoroughly mixed and pressed into pellets. The pellets were placed into separate fused silica tubes that were evacuated and sealed. Each tube was heated to 570 °C (500 °C for $CsYTe_3O_8$) for 48 h with intermediate regrinding. The powder X-ray diffraction (PXRD) patterns of the resultant polycrystalline products were in good agreement with the calculated patterns from the single crystal data (Supporting Information).

Single Crystal X-ray Diffraction. To determine the crystal structures of all four tellurites, standard crystallographic methods were used. A colorless block ($0.023 \times 0.026 \times 0.042$ mm^3) for $NaYTe_4O_{10}$, a colorless rod ($0.015 \times 0.025 \times 0.041$ mm^3) for $KY(TeO_3)_2$, a colorless rod ($0.021 \times 0.031 \times 0.034$ mm^3) for $RbY(TeO_3)_2$, and a colorless hexagonal plate ($0.018 \times 0.034 \times 0.037$ mm^3) for $CsYTe_3O_8$ were used for single crystal data analyses. All data were obtained using a Bruker SMART BREEZE diffractometer equipped with a 1K CCD area detector using graphite monochromated Mo Kα radiation at room temperature. A hemisphere of data was collected using a narrow-frame method with an exposure time of 10 s/frame and scan widths of 0.30° in omega. To monitor crystal and instrument stability, the first 50 frames were remeasured at the end of the data collection. The maximum correction applied to the intensities was less than 1%. The data were integrated using the SAINT program,[12] with the intensities corrected for Lorentz factor, polarization, air absorption, and absorption attributed to the variation in the path length through the detector faceplate. A semiempirical absorption correction was made on the hemisphere of data with the SADABS program.[13] The data were solved using SHELXS-97[14] and refined with SHELXL-97.[15] All calculations were performed using the WinGX-98 crystallographic software package.[16] Crystallographic data and selected bond distances for all four reported materials are listed in Tables 1 and 2, respectively.

Powder X-ray Diffraction (PXRD). PXRD patterns were obtained on a Bruker D8-Advance diffractometer using Cu Kα radiation at room temperature with 40 kV and 40 mA. The well-ground samples were mounted on sample holders and scanned in the 2θ range of 5–70° with a step size of 0.02° and a step time of 0.2 s. PXRD patterns can be found in the Supporting Information.

Table 1. Crystallographic Data for $NaYTe_4O_{10}$, $KY(TeO_3)_2$, $RbY(TeO_3)_2$, and $CsYTe_3O_8$

	$NaYTe_4O_{10}$	$KYTe_2O_6$	$RbYTe_2O_6$	$CsYTe_3O_8$
fw	782.30	479.21	525.58	732.62
space group	*P*42/*nbc* (No. 133)	*Pnma* (No. 62)	*Pnma* (No. 62)	$R\bar{3}$ (No. 148)
a (Å)	8.9337(2)	13.563(10)	13.7281(3)	7.3766(10)
b (Å)	8.9337(2)	5.9911(10)	6.0414(2)	7.3766(10)
c (Å)	13.4854(3)	8.5601(10)	8.6320(2)	28.933(6)
V (Å^3)	1076.28(5)	695.6(5)	715.91(3)	1363.4(5)
Z	4	4	4	6
T (K)	298.0(2)	298.0(2)	298.0(2)	298.0(2)
λ (Å)	0.71073	0.71073	0.71073	0.71073
$R(F)^a$	0.0146	0.0233	0.0184	0.0455
$R_w(F_o^2)^b$	0.0351	0.0461	0.0401	0.1086

$^aR(F) = \sum||F_o| - |F_c||/\sum|F_o|$. $^bR_w(F_o^2) = [\sum w(F_o^2 - F_c^2)^2/\sum w(F_o^2)^2]^{1/2}$.

Infrared (IR) Spectroscopy. IR spectra were recorded on a Thermo Scientific Nicolet 6700 FT-IR spectrometer in the spectral range of 400–4000 cm^{-1}. The samples were ground with KBr matrixes for the measurements.

UV–Vis Diffuse Reflectance Spectroscopy. UV–vis diffuse reflectance spectra were obtained on a Varian Cary 500 scan UV–vis–NIR spectrometer at the Korea Photonics Technology Institute over the spectral range of 200–2500 nm at room temperature. Reflectance spectra were transformed to absorbance data using the Kubelka–Munk function.[17]

Thermogravimetric Analysis (TGA). TGA was performed on a Setaram LABSYS TG-DTA thermogravimetric analyzer. The well-ground samples were mounted within alumina crucibles and heated to 1000 °C at 10 °C min^{-1} under flowing argon.

Scanning Electron Microscopy/Energy Dispersive Analysis by X-ray (SEM/EDAX). A Hitachi S-3400N/Horiba Energy EX-250 instrument was utilized to perform SEM/EDAX. EDAX for $NaYTe_4O_{10}$, $KY(TeO_3)_2$, $RbY(TeO_3)_2$, and $CsYTe_3O_8$ reveals A/Y/Te ratios of 1.0:1.1:4.1, 1.0:1.0:1.9, 1.0:0.9:2.0, and 1.0:1.0:3.0, respectively.

RESULTS AND DISCUSSION

$NaYTe_4O_{10}$ Structure. $NaYTe_4O_{10}$ is a new quaternary sodium yttrium tellurite that crystallizes in the highly symmetric tetragonal space group *P*42/*nbc* (No. 133). The structure of $NaYTe_4O_{10}$ is composed of YO_8 square antiprisms and TeO_4 seesaws. The unique Y^{3+} cation is connected to eight oxygen atoms with Y–O bond distances and O–Y–O bond angles ranging from 2.345(2) to 2.372(2) Å and from 68.05(10) to 144.51(10)°, respectively. Within an asymmetric unit, the unique Te^{4+} cation also exists and makes bonds with four oxygen atoms. The Te^{4+} cation exhibits three normal Te–O bond distances [1.856(2)–1.9581(11) Å] and one very long [2.514(2) Å] Te–O bond distance. In addition, the observed O–Te–O bond angles range from 75.23(9) to 163.50(5)°. There are two different kinds of coordination modes for four-coordinate tellurites: one environment has two shorter and two longer Te–O bond lengths, and the other exhibits three shorter Te–O bond distances and one very long Te–O bond distance.[3h] The variable coordination geometries for TeO_4 polyhedra are considered to be the flexibility demonstrated by the Te^{4+} cation. On the basis of the stereoactive lone pair, the coordination environment around the Te^{4+} cation is asymmetric. Finally, the Na^+ cation is in a six-coordinate environment with oxygen atoms, where the Na–O contacts range from 2.278(2) to 2.570(3) Å. As seen in Figure

dx.doi.org/10.1021/ic502724n | Inorg. Chem. 2015, 54, 389–395

Table 2. Selected Bond Distances (Å) for $NaYTe_4O_{10}$, $KY(TeO_3)_2$, $RbY(TeO_3)_2$, and $CsYTe_3O_8$

$NaYTe_4O_{10}$		$KY(TeO_3)_2$		$RbY(TeO_3)_2$		$CsYTe_3O_8$	
Y(1)−O(1) × 4	2.345(2)	Y(1)−O(1) × 2	2.267(3)	Y(1)−O(1) × 2	2.267(2)	Y(1)−O(1) × 6	2.252(9)
Y(1)−O(2) × 4	2.372(2)	Y(1)−O(2)	2.272(4)	Y(1)−O(2)	2.273(3)	Y(1)−O(2) × 6	2.290(9)
Te(1)−O(1)	1.856(2)	Y(1)−O(3) × 2	2.240(3)	Y(1)−O(3) × 2	2.2515(19)	Te(1)−O(1)	1.838(8)
Te(1)−O(2)	1.861(2)	Y(1)−O(4)	2.236(4)	Y(1)−O(4)	2.237(3)	Te(1)−O(2)	1.871(9)
Te(1)−O(2)	2.514(2)	Te(1)−O(1) × 2	1.847(3)	Te(1)−O(1) × 2	1.8513(19)	Te(1)−O(3)	2.158(3)
Te(1)−O(3)	1.9581(11)	Te(1)−O(2)	1.866(4)	Te(1)−O(2)	1.871(3)	Te(1)−O(4)	2.166(2)
Na(1)−O(1) × 4	2.278(2)	Te(2)−O(3) × 2	1.855(3)	Te(2)−O(3) × 2	1.8530(18)	Cs(1)−O(1) × 3	3.104(8)
Na(1)−O(3) × 2	2.570(3)	Te(2)−O(4)	1.858(4)	Te(2)−O(4)	1.856(3)	Cs(1)−O(1) × 3	3.698(10)
		K(1)−O(1) × 2	3.020(3)	Rb(1)−O(1) × 2	3.037(2)	Cs(1)−O(1) × 2	3.787(10)
		K(1)−O(2) × 2	3.0707(10)	Rb(1)−O(2) × 2	3.0959(7)	Cs(1)−O(2) × 3	3.260(10)
		K(1)−O(3) × 2	2.821(3)	Rb(1)−O(3) × 2	2.943(2)	Cs(1)−O(3)	3.377(15)
		K(1)−O(3) × 2	2.872(3)	Rb(1)−O(3) × 2	2.949(2)		

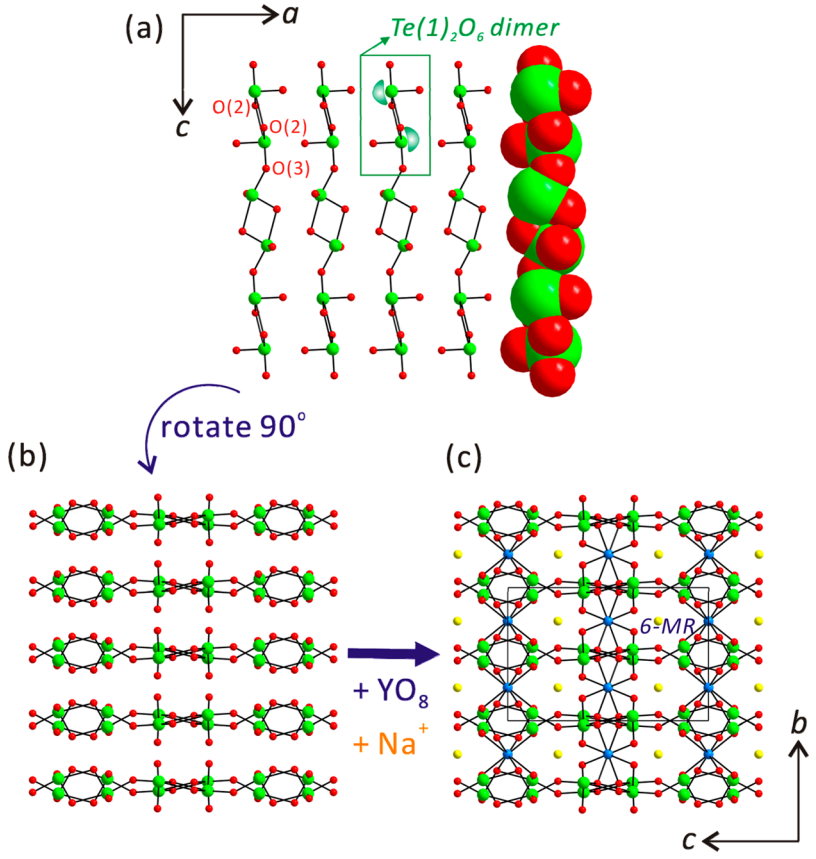

Figure 1. Ball-and-stick and space-filling representations of $NaYTe_4O_{10}$ (yellow, Na; blue, Y; green, Te; red, O). (a and b) Infinite unidimensional helical chains composed of edge- and corner-shared TeO_4 polyhedra are observed along the [001] direction. (c) YO_8 square antiprisms are linked to the chains and form a highly symmetric three-dimensional framework. Six-membered ring (6-MR) channels running along the [100] direction are observed from the three-dimensional framework.

1a, each $Te(1)O_4$ distorted seesaw shares its edge through two O(2) atoms and forms $Te(1)_2O_6$ dimers. The $Te(1)_2O_6$ dimers further share their corners through O(3) and generate infinite unidimensional chains along the approximate [001] direction (Figure 1a and b). Interestingly, each edge-sharing $Te(1)_2O_6$ dimer is oriented perpendicularly within a chain, which results in a helical chain structure (see the space-filling model in Figure 1a). The alternating alignment of $Te(1)_2O_6$ dimers may be attributable to the stereoactive lone pairs on Te^{4+} cations. Then, YO_8 square antiprisms are linked to the chains of TeO_4 polyhedra through O(1) and O(2) to form a highly symmetric three-dimensional framework (Figure 1c) in which the YO_8 groups serve as interchain linkers. The three-dimensional framework of $NaYTe_4O_{10}$ contains six-membered ring (6-MR) channels running along the [100] direction (Figure 1c). Within the 6-MR channels, Na^+ cations reside and interact with six oxygen atoms. Six- and eight-membered ring channels also run along the [010] and [001] directions, respectively (Figure 2). In terms of connectivity, the crystal structure of $NaYTe_4O_{10}$ can be written as an anionic framework of $\{[Y(1)O_{4/2}O_{4/3}]^{-3.667}4[Te(1)O_{2/2}O_{2/3}]^{+0.667}\}^-$. Charge neutrality is maintained through the Na^+ cation. Bond valence sum calculations[18] for Y^{3+}, Te^{4+}, and O^{2-} result in values of 3.17, 3.96, and 1.98−2.14, respectively.

$AY(TeO_3)_2$ (A = K and Rb). The new isostructural alkali metal yttrium tellurites $KY(TeO_3)_2$ and $RbY(TeO_3)_2$ reveal

dx.doi.org/10.1021/ic502724n | Inorg. Chem. 2015, 54, 389−395

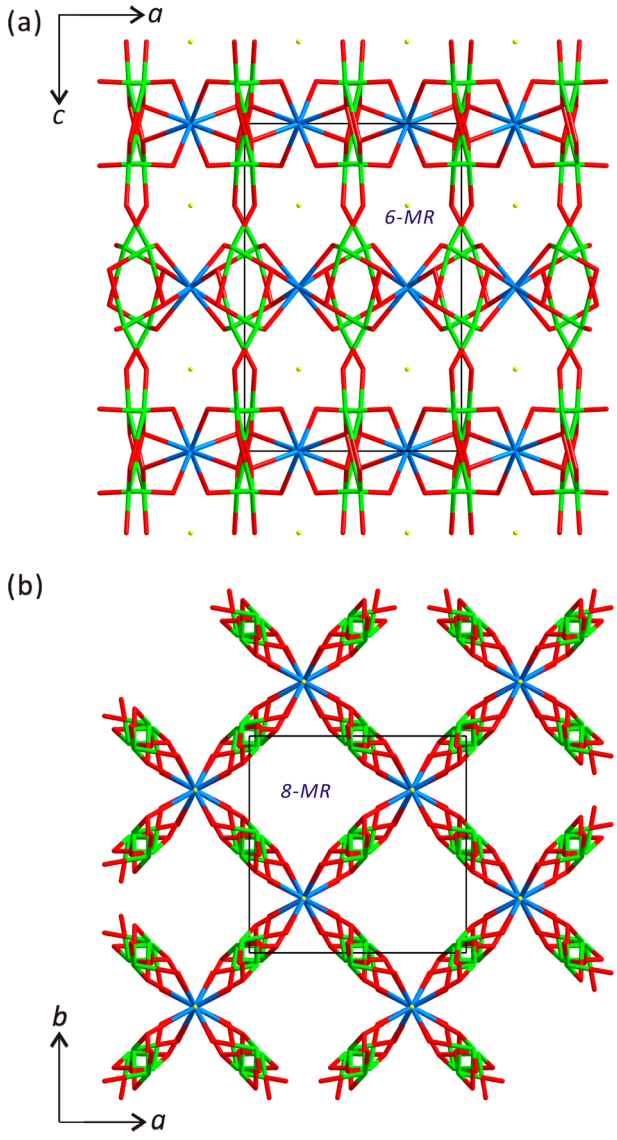

Figure 2. Wire representations of $NaYTe_4O_{10}$ in the (a) *ac* plane and (b) *ab* plane (yellow, Na; blue, Y; green, Te; red, O). Six- (6-MR) and eight-membered ring (8-MR) channels run along the [010] and [001] directions, respectively.

framework structures similar to those of their selenium analogues $KY(SeO_3)_2$ and $RbY(SeO_3)_2$.[19] Therefore, a brief structural description for $KY(TeO_3)_2$ will be provided. $KY(TeO_3)_2$ crystallizes in the orthorhombic space group *Pnma* (No. 62) and exhibits a three-dimensional framework structure containing YO_6 octahedra and TeO_3 trigonal pyramids. The bond distances for Y−O in the distorted YO_6 octahedra range from 2.236(4) to 2.272(4) Å, whereas the O−Y−O bond angles vary from 87.50(16) to 177.15(16)°. There are two unique Te^{4+} cations within an asymmetric unit, in which the Te−O bond lengths and the O−Te−O bond angles range from 1.847(3) to 1.866(4) Å and from 96.61(13) to 101.3(2)°, respectively. The alkali metal cation K^+ is in eight-coordinate environment with oxygen atoms in which the K−O contact distances range from 2.821(3) to 3.0707(10) Å. The corner sharing between each YO_6 octahedron and TeO_3 trigonal pyramid through oxygen atoms results in a three-dimensional framework structure (Figure 3). Four-membered ring channels that are running in

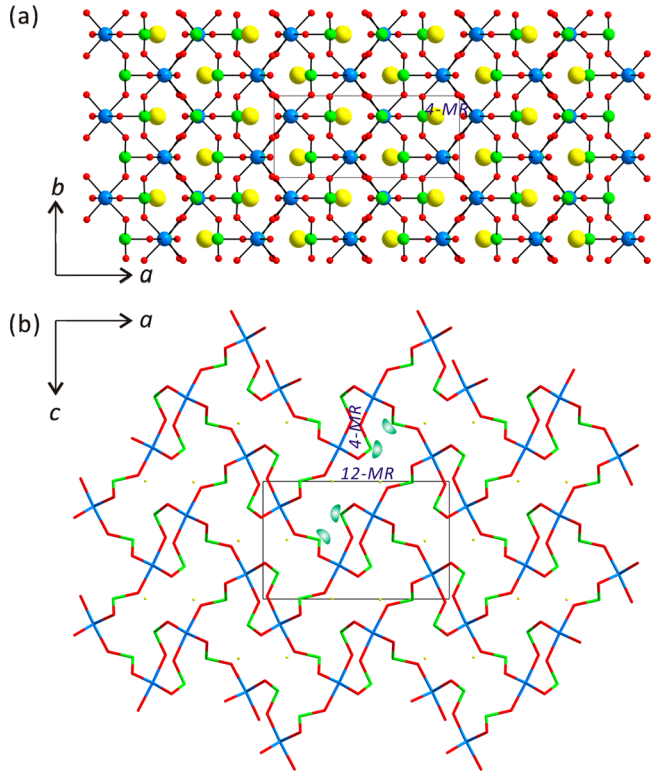

Figure 3. (a) Ball-and-stick representation of $KY(TeO_3)_2$ in the *ab* plane. Four-membered ring (4-MR) channels running down the [001] direction are observed. (b) Wire model of $KY(TeO_3)_2$ in the *ac* plane, in which both four- and 12-membered ring channels are observed along the [010] direction. Yellow, K; blue, Y; green, Te; red, O.

the [001] direction are observed in the *ab* plane (Figure 3a). In addition, four- and 12-membered ring channels are found along the [010] direction in the *ac* plane (Figure 3b). Lone pairs on the TeO_3 trigonal pyramids direct inwardly within the larger 12-MR channels. The alkali metal cation K^+ also resides in the 12-MR channels. The connectivity of $KY(TeO_3)_2$ can be described as an anionic framework of $\{[YO_{6/2}]^{3-}\ 2[TeO_{3/2}]^+\}^-$, with charge neutrality retained by the K^+ cation within the channel. Bond valence sums[18] for K^+, Te^{4+}, Y^{3+}, and O^{2-} are calculated to be 0.89, 3.97−4.00, 2.97, and 1.93−2.05, respectively.

$CsYTe_3O_8$. Another new quaternary alkali metal tellurite, $CsYTe_3O_8$, crystallizes in the trigonal space group $R\bar{3}$ (No. 148). $CsYTe_3O_8$ reveals a three-dimensional framework structure that consists of YO_6 and TeO_4 polyhedra. Two unique Y^{3+} cations, $Y(1)^{3+}$ and $Y(2)^{3+}$, exist in the octahedral coordination environment with Y−O bond lengths of 2.252(9) and 2.290(9) Å, respectively. The unique Te^{4+} cation is connected to four oxygen atoms in a seesaw moiety with Te−O bond distances of 1.838(8)−2.166(2) Å. The coordination environment of the Te^{4+} cation is asymmetric due to the lone pair on the cation. Huge Cs^+ cations remaining between the framework interact with 12 oxygen atoms with Cs−O contact lengths of 3.104(8)−3.787(10) Å. The most interesting structural feature of $CsYTe_3O_8$ is the layered backbone consisting of TeO_4 polyhedra (Figure 4a). As seen in Figure 4a, the layer found in $CsYTe_3O_8$ is composed of six-membered rings containing corner-shared TeO_4 seesaws in alternating directions. Three lone pairs direct inwardly and three point outwardly in the 6-MRs. A similar alternating arrangement of

dx.doi.org/10.1021/ic502724n | *Inorg. Chem.* 2015, 54, 389−395

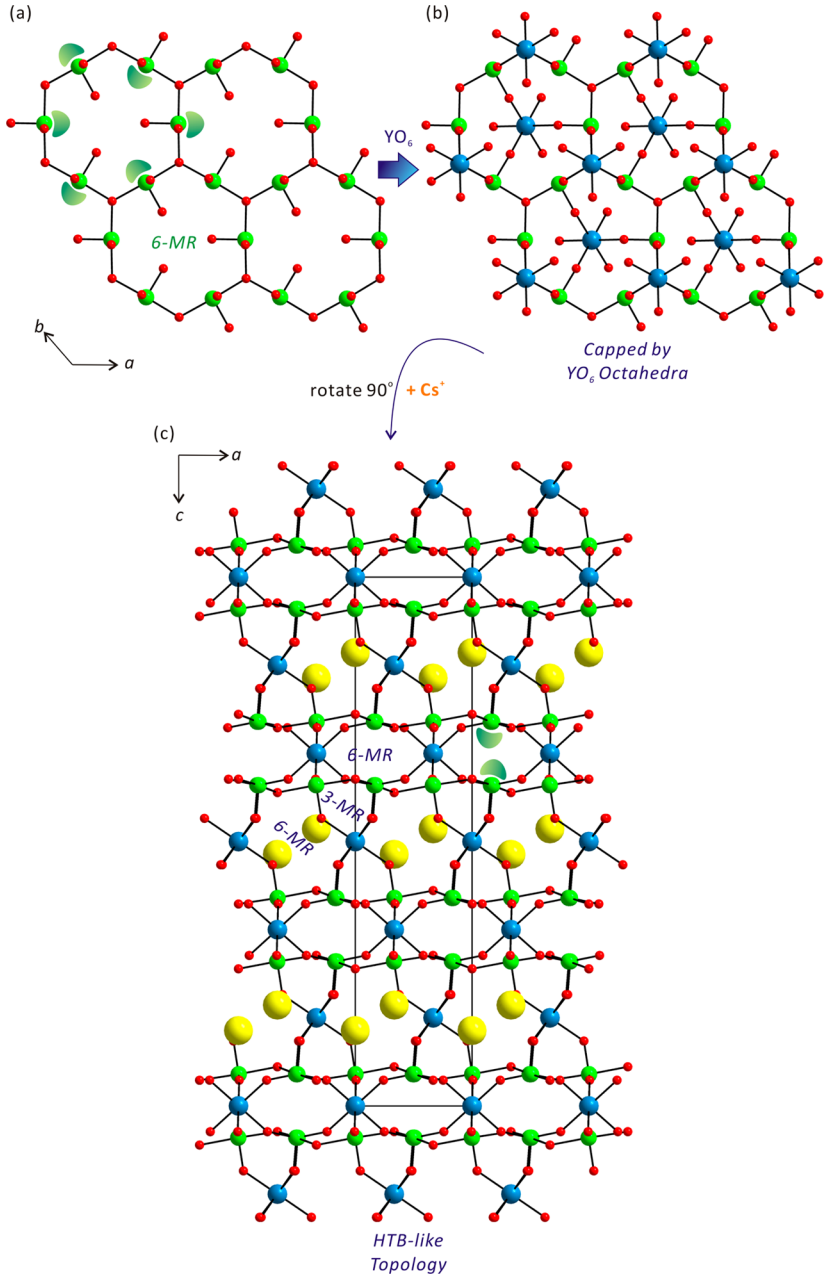

Figure 4. (a) Ball-and-stick representation of TeO_4 6-MRs in $CsYTe_3O_8$ in the *ab* plane. The lone pairs are shown schematically. (b) The oxide layer is capped by YO_6 octahedra from above and below. (c) An HTB-like topology that is composed of HTO-like layers of TeO_4 polyhedra and YO_6 octahedral linkers is observed in the *ac* plane, in which 3-MR, smaller 6-MR, and larger 6-MR channels are observed along the [010] direction. Yellow, Cs; blue, Y; green, Te; red, O.

lone pairs and oxide anions has been observed from HTO-like layers of corner-shared IO_5 polyhedra in α-$Cs_2I_4O_{11}$.[20] The oxide layer is capped by $Y(1)O_6$ octahedra along the [001] direction. It should be noted that capping of the HTO layers on one or both sides is normally observed from tellurite, selenite, and methyl phosphonate groups. In addition, further interlayer connections are made by linking $Y(2)O_6$ octahedra along the [001] direction. Thus, both Y(1)O6 and Y(2)O6 serve as interlayer linkers, which results in a three-dimensional framework. More specifically, $CsYTe_3O_8$ is the first example exhibiting HTB-like topology that is composed of HTO-like layers of TeO_4 polyhedra and YO_6 octahedral linkers. Within the framework of $CsYTe_3O_8$, 3-MR, smaller 6-MR, and larger 6-MR channels are observed along the [010] direction (Figure 4c). As shown in Figure 4c, Cs^+ cations reside in the larger 6-MR channels attributable to the lone pairs on the TeO_4 polyhedra that point within the smaller 6-MR channels. As can be seen in Figure 5, two main topological differences differentiate HTB and $CsYTe_3O_8$. First, the structural backbone of HTB consists of a hexagonal network of corner-shared MO_6 octahedra, whereas that of $CsYTe_3O_8$ is composed of an HTO-like layer of corner-shared TeO_4 polyhedra. Second, while smaller 3-MR and larger 6-MR channels containing the "A" cation are observed along the [001] direction in HTB, similar channels are not found along the same direction in $CsYTe_3O_8$ because the HTO-like layers are capped by YO_6 octahedra from above and below. In terms of connectivity, the backbone of $CsYTe_3O_8$ can be represented as an anionic framework of

dx.doi.org/10.1021/ic502724n | *Inorg. Chem.* 2015, 54, 389−395

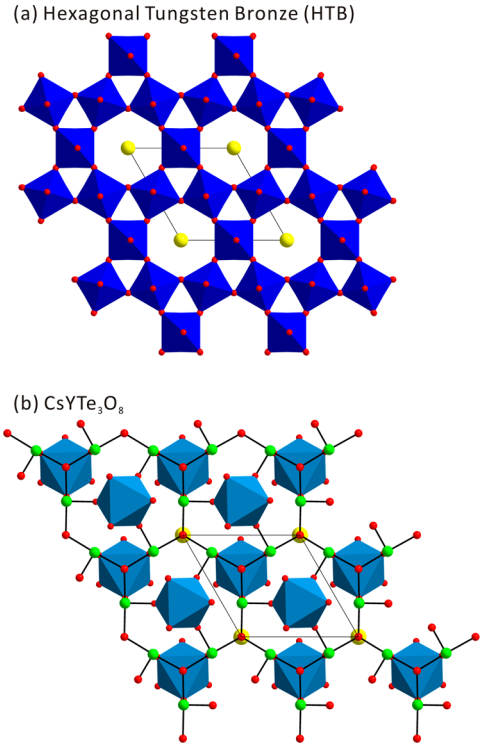

Figure 5. Ball-and-stick and polyhedral representations of (a) HTB topology and (b) $CsYTe_3O_8$. Yellow, alkali metal or Cs; blue, W or Y; green, Te; red, O.

$\{[YO_{6/2}]^{-3}\ 3[TeO_{2/2}O_{2/3}]^{+0.667}\}^{-1}$ with the charge balance maintained by the Cs^+ cation. Bond valence sum calculations[18] for Cs^+, Y^{3+}, and Te^{4+} result in values of 0.94, 2.73–3.02, and 3.88, respectively.

Cation Size Effect. Although crystals of all four reported materials have been grown under similar hydrothermal reaction conditions, the crystal structures are quite different. Because the materials are not stoichiometrically equivalent, it is difficult to compare the frameworks directly. However, it is obvious that the alkali metal cations play important roles in determining the framework structures of the products. The observed coordination numbers for Na^+, K^+ (or Rb^+), and Cs^+ in $NaYTe_4O_{10}$, $KY(TeO_3)_2$ [or $RbY(TeO_3)_2$], and $CsYTe_3O_8$ are 6, 8, and 12, respectively. The different coordination numbers arising from the size differences of the cations influence channel geometries and their subsequent stoichiometries.

Infrared (IR) Spectroscopy. The IR spectra for $NaYTe_4O_{10}$, $KY(TeO_3)_2$, $RbY(TeO_3)_2$, and $CsYTe_3O_8$ reveal distinctive Y–O vibrations ranging from approximately 399 to 410 cm^{-1}. Indicative vibrations arising from Te–O bonds are also monitored at approximately 647–805 cm^{-1}. The IR assignments agree well with those reported for oxides containing Y^{3+} and Te^{4+} cations.[3h,10,21] The IR spectra for all four reported compounds are provided in the Supporting Information.

UV–Vis Diffuse Reflectance Spectroscopy. To calculate the band gaps of the reported materials, UV–vis diffuse reflectance spectra were utilized. The absorption data (K/S) were calculated after obtaining the spectra through the following Kubelka–Munk function[17]

$$F(R) = \frac{(1-R)^2}{2R} = \frac{K}{S}$$

where K, S, and R are the absorption, scattering, and reflectance, respectively. Once the linear portions of the rising curves in the K/S versus E plots are extrapolated to zero, the absorptions begin at approximately 3.9, 3.8, 3.6, and 3.4 eV for $NaYTe_4O_{10}$, $KY(TeO_3)_2$, $RbY(TeO_3)_2$, and $CsYTe_3O_8$, respectively. The observed band gaps may be due to distortions arising from the asymmetric TeO_3 and TeO_4 groups, as well as interactions of Te–O bonds. The UV–vis diffuse reflectance spectra for all four compounds can be found in the Supporting Information.

Thermogravimetric Analysis (TGA). To examine the thermal behavior and stability of the reported materials, TGA and PXRD conducted at different temperatures have been employed. The TGA diagrams reveal that no weight losses occur up to 700, 810, 800, and 790 °C for $NaYTe_4O_{10}$, $KY(TeO_3)_2$, $RbY(TeO_3)_2$, and $CsYTe_3O_8$, respectively. PXRD data measured at different temperatures confirm the thermal stabilities of the oxide materials. Above these temperatures, each material begins to decompose thermally. The PXRD patterns measured after calcination at 1000 °C show that the materials decompose to mixtures of $Y_2Te_4O_{11}$ (PDF: 35-1162) and some amorphous phases containing the corresponding alkali metal cations. The TGA data and PXRD patterns measured at different temperatures are found in the Supporting Information.

Dipole Moment Calculations. Because all four reported materials accommodate polyhedra of local unsymmetrical environments such as TeO_3 and TeO_4, it is worthwhile to determine the extent of distortions for the groups. By doing so, we can better understand extended frameworks with asymmetric environments. The unsymmetrical coordination environment for the constituent polyhedra has been quantified by calculating the local dipole moments through a bond valence sum approach.[22] The calculated local dipole moments in the $NaYTe_4O_{10}$, $KY(TeO_3)_2$, $RbY(TeO_3)_2$, and $CsYTe_3O_8$ groups for TeO_3 and TeO_4 are 8.3–8.8 and 6.1–10.3 D (debyes), respectively (Table 3). The values are quite close to the local dipole moments for TeO_3 and TeO_4 polyhedra found from previously published mixed-metal tellurium oxides.[3h,6c,23]

Table 3. Calculation of Dipole Moments for TeO_3 and TeO_4 Polyhedra in $NaYTe_4O_{10}$, $KY(TeO_3)_2$, $RbY(TeO_3)_2$, and $CsYTe_3O_8$

compound	species	dipole moment (D)
$NaYTe_4O_{10}$	$Te(1)O_4$	10.3
$KY(TeO_3)_2$	$Te(1)O_3$	8.6
	$Te(2)O_3$	8.8
$RbY(TeO_3)_2$	$Te(1)O_3$	8.3
	$Te(2)O_3$	8.4
$CsYTe_3O_8$	$Te(1)O_4$	6.1

CONCLUSIONS

Crystals and bulk phases of four novel alkali metal yttrium tellurite materials, $NaYTe_4O_{10}$, $KY(TeO_3)_2$, $RbY(TeO_3)_2$, and $CsYTe_3O_8$, have been synthesized, and their crystal structures were determined through X-ray diffraction analyses. Highly symmetric $NaYTe_4O_{10}$ shows a 3D framework composed of YO_8 square antiprisms and TeO_4 seesaws. Isostructural $KY(TeO_3)_2$ and $RbY(TeO_3)_2$ exhibit another 3D framework containing YO_6 octahedra and TeO_3 trigonal pyramids. $CsYTe_3O_8$ reveals a novel variant of HTB topology consisting

dx.doi.org/10.1021/ic502724n | Inorg. Chem. 2015, 54, 389–395

of YO_6 octahedra and HTO-like layers of TeO_4 seesaws. UV−vis diffuse reflectance spectra indicate that $NaYTe_4O_{10}$, $KY(TeO_3)_2$, $RbY(TeO_3)_2$, and $CsYTe_3O_8$ have band gaps of 3.9, 3.8, 3.6, and 3.4 eV, respectively. IR spectra for all materials display specific vibrations for Y−O and Te−O bonds. Although the reported compounds are thermally stable up to 700−810 °C, they decompose to mixtures of $Y_2Te_4O_{11}$ and some amorphous phases above these temperatures. Further syntheses of novel mixed-metal tellurites with asymmetric environments are ongoing, and the experimental results will be introduced shortly.

■ ASSOCIATED CONTENT

Supporting Information

X-ray crystallographic files in CIF format, calculated and observed powder X-ray diffraction patterns, IR spectra, UV−vis diffuse reflectance spectra, and thermogravimetric analysis diagrams for $NaYTe_4O_{10}$, $KY(TeO_3)_2$, $RbY(TeO_3)_2$, and $CsYTe_3O_8$. This material is available free of charge via the Internet at http://pubs.acs.org.

■ AUTHOR INFORMATION

Corresponding Author

*E-mail: kmok@cau.ac.kr. Phone: +82-2-820-5197. Fax: +82-2-825-4736.

Notes

The authors declare no competing financial interest.

■ ACKNOWLEDGMENTS

This research was supported by the Chung-Ang University Research Scholarship Grant in 2013. This research was also supported by a National Research Foundation (NRF) of Korea grant (MSIP, 2014M3A9B8023478) funded by the Korean government.

■ REFERENCES

(1) West, A. R. *Solid State Chemistry and Its Applications*; John Wiley & Sons: New York, 1984.

(2) (a) Alonso, J. A.; Castro, A.; Puebla, E. G.; Monge, M. A.; Rasines, I.; Valero, C. R. *J. Solid State Chem.* **1987**, *69*, 36−42. (b) Champarnaud-Mesjard, J. C.; Frit, B.; Chagraoui, A.; Tairi, A. *J. Solid State Chem.* **1996**, *127*, 248−255. (c) *CRC Handbook of Chemistry and Physics*, internet version 2005; Lide, D. R., Ed.; CRC Press: Boca Raton, FL, 2005.

(3) (a) Alcock, N. W.; Harrison, W. D. *Acta Crystallogr.* **1982**, *B38*, 1809−1811. (b) Tagg, S. L.; Huffman, J. C.; Zwanziger, J. W. *Chem. Mater.* **1994**, *6*, 1884−1889. (c) Tagg, S. L.; Huffman, J. C.; Zwanziger, J. W. *Acta Chem. Scand.* **1997**, *51*, 118−121. (d) Mayer, H.; Weil, M. *Z. Anorg. Allg. Chem.* **2003**, *629*, 1068−1072. (e) Jiang, H.; Ma, E.; Mao, J.-G. *Inorg. Chem.* **2007**, *46*, 7012−7023. (f) Kong, F.; Hu, C.; Hu, T.; Zhou, Y.; Mao, J.-G. *Dalton Trans.* **2009**, 4962−4970. (g) Kim, M. K.; Kim, S.-H.; Chang, H.-Y.; Halasyamani, P. S.; Ok, K. M. *Inorg. Chem.* **2010**, *49*, 7028−7034. (h) Lee, D. W.; Oh, S.-J.; Halasyamani, P. S.; Ok, K. M. *Inorg. Chem.* **2011**, *50*, 4473−4480. (i) Kim, Y. H.; Lee, D. W.; Ok, K. M. *Inorg. Chem.* **2014**, *53*, 1250−1256.

(4) (a) Opik, U.; Pryce, M. H. L. *Proc. R. Soc. London* **1957**, *A238*, 425−447. (b) Bader, R. F. W. *Can. J. Chem.* **1962**, *40*, 1164−1175. (c) Pearson, R. G. *J. Am. Chem. Soc.* **1969**, *91*, 4947−4955. (d) Pearson, R. G. *J. Mol. Struct.: THEOCHEM* **1983**, *103*, 25−34. (e) Wheeler, R. A.; Whangbo, M.-H.; Hughbanks, T.; Hoffmann, R.; Burdett, J. K.; Albright, T. A. *J. Am. Chem. Soc.* **1986**, *108*, 2222−2236. (f) Oh, S.-J.; Lee, D. W.; Ok, K. M. *Inorg. Chem.* **2012**, *51*, 5393−5399.

(5) (a) Nye, J. F. *Physical Properties of Crystals*; Oxford University Press: Oxford, U.K., 1957. (b) Jona, F.; Shirane, G. *Ferroelectric Crystals*; Pergamon Press: Oxford, U.K., 1962. (c) Cady, W. G. *Piezoelectricity: An Introduction to the Theory and Applications of Electromechanical Phenomena in Crystals*; Dover: New York, 1964. (d) Lang, S. B. *Sourcebook of Pyroelectricity*; Gordon & Breach Science: London, 1974. (e) Ok, K. M.; Chi, E. O.; Halasyamani, P. S. *Chem. Soc. Rev.* **2006**, *35*, 710−717.

(6) (a) Jiang, H.; Huang, S.; Fan, Y.; Mao, J.; Cheng, W. *Chem.−Eur. J.* **2008**, *14*, 1972−1981. (b) Zhang, S.; Jiang, H.; Sun, C.; Mao, J. G. *Inorg. Chem.* **2009**, *48*, 11809−11820. (c) Kim, Y. H.; Lee, D. W.; Ok, K. M. *Inorg. Chem.* **2014**, *53*, 5240−5245.

(7) (a) Magneli, A. *Acta Chem. Scand.* **1951**, *5*, 670−672. (b) Magneli, A. *Acta Chem. Scand.* **1953**, *7*, 315−324. (c) Goodman, P. *Acta Crystallogr.* **1976**, *B32*, 3280−3285. (d) Galasso, F.; Darby, W. *J. Phys. Chem.* **1964**, *68*, 1253−1261. (e) Hussain, A.; Kihlborg, L.; Klug, A. *J. Solid State Chem.* **1978**, *25*, 189−195. (f) Kudo, T.; Oi, J.; Kishimoto, A.; Inoue, H. *Solid State Ionics* **1990**, *40/41*, 567−571.

(8) (a) Harrison, W. T. A.; Dussack, L. L.; Jacobson, A. J. *Inorg. Chem.* **1994**, *33*, 6043−6049. (b) Vaughey, J. T.; Harrison, W. T. A.; Dussack, L. L.; Jacobson, A. J. *Inorg. Chem.* **1994**, *33*, 4370−4375. (c) Harrison, W. T. A.; Dussack, L. L.; Jacobson, A. J. *Inorg. Chem.* **1995**, *34*, 4774−4779. (d) Harrison, W. T. A.; Dussack, L. L.; Jacobson, A. J. *Inorg. Chem.* **1996**, *35*, 1461−1467. (e) Balraj, V.; Vidyasagar, K. *Inorg. Chem.* **1998**, *37*, 4764−4774.

(9) Hoess, P.; Osvet, A.; Meister, F.; Batentschuk, M.; Winnacker, A.; Schleid, T. *J. Solid State Chem.* **2008**, *181*, 2783−2788.

(10) Bang, S.-e.; Pan, Z.; Kim, Y. H.; Lee, D. W.; Ok, K. M. *J. Solid State Chem.* **2013**, *208*, 65−70.

(11) Zitzer, S.; Schleifenbaum, F.; Schleid, T. *Z. Naturforsch.* **2014**, *B69*, 150−158.

(12) *SAINT*, version 4.05; Siemens Analytical X-ray Instruments: Madison, WI, 1995; a program for area detector absorption correction.

(13) Blessing, R. H. *Acta Crystallogr.* **1995**, *A51*, 33−38.

(14) Sheldrick, G. M. *SHELXS-97*; University of Goettingen: Goettingen, Germany, 1997; a program for automatic solution of crystal structures.

(15) Sheldrick, G. M. *SHELXL-97*; University of Goettingen: Goettingen, Germany, 1997; a program for crystal structure refinement.

(16) Farrugia, L. J. *J. Appl. Crystallogr.* **1999**, *32*, 837−838.

(17) (a) Kubelka, P.; Munk, F. *Z. Tech. Phys.* **1931**, *12*, 593. (b) Tauc, J. *Mater. Res. Bull.* **1970**, *5*, 721−729.

(18) (a) Brown, I. D.; Altermatt, D. *Acta Crystallogr.* **1985**, *B41*, 244−247. (b) Brese, N. E.; O'Keeffe, M. *Acta Crystallogr.* **1991**, *B47*, 192−197.

(19) Bang, S.-e.; Lee, D. W.; Ok, K. M. *Inorg. Chem.* **2014**, *53*, 4756−4762.

(20) Ok, K. M.; Halasyamani, P. S. *Angew. Chem., Int. Ed.* **2004**, *43*, 5489−5491.

(21) (a) Lee, D. W.; Ok, K. M. *Inorg. Chem.* **2013**, *52*, 6236−6238. (b) Raju, K. V.; Raju, C. N.; Sailaja, S.; Dhoble, S. J.; Reddy, B. S. *J. Lumin.* **2013**, *134*, 297−302.

(22) (a) Galy, J.; Meunier, G. *J. Solid State Chem.* **1975**, *13*, 142−159. (b) Maggard, P. A.; Nault, T. S.; Stern, C. L.; Poeppelmeier, K. R. *J. Solid State Chem.* **2003**, *175*, 27−33. (c) Izumi, H. K.; Kirsch, J. E.; Stern, C. L.; Poeppelmeier, K. R. *Inorg. Chem.* **2005**, *44*, 884−895.

(23) Bae, S.-w.; Kim, C.-Y.; Lee, D. W.; Ok, K. M. *Inorg. Chem.* **2014**, *53*, 11328−11334.